

A new model for the vertical spectral diffuse attenuation coefficient of downwelling irradiance in turbid coastal waters: validation with *in situ* measurements

Arthi Simon and Palanisamy Shanmugam*

Ocean Optics and Imaging Laboratory, Department of Ocean Engineering, Indian Institute of Technology Madras,
Chennai-600036, India
*pshanmugam@iitm.ac.in

Abstract: The vertical spectral diffuse attenuation coefficient of K_d is an important optical property related to the penetration and availability of light underwater, which is of fundamental interest in studies of ocean physics and biology. Models developed in the recent decades were mainly based on theoretical analyses and numerical (radiative transfer) simulations to estimate this property in optically deep waters, thus leaving inadequate knowledge of its variability at multiple depths and wavelengths, covering a wide range of solar incident geometry, in turbid coastal waters. In the present study, a new model is developed to quantify the vertical, spatial and temporal variability of K_d at multiple wavelengths and to quantify its dependence with respect to solar incident geometry under differing sky conditions. Thus, the new model is derived as a function of inherent optical properties (IOPs – absorption a and backscattering b_b), solar zenith angle and depth parameters. The model results are rigorously evaluated using time-series and discrete *in situ* data from clear and turbid coastal waters. The K_d values derived from the new model are found to agree with measured data within the mean relative error 0.02~6.24% and R^2 0.94~0.99. By contrast, the existing models have large errors when applied to the same data sets. Statistical results of the new model for the vertical spectral distribution of K_d in clear oceanic waters (for different solar zenith and in-water conditions) are also good when compared to those of the existing models. These results suggest that the new model can provide an improved interpretation about the variation of the vertical spectral diffuse attenuation coefficient of downwelling irradiance, which will have important implications for ocean physics, biogeochemical cycles and underwater applications in both relatively clear and turbid coastal waters.

©2013 Optical Society of America

OCIS codes: (010.4450) Oceanic optics; (010.1350) Backscattering; (290.5850) Scattering, particles.

References and links

1. N. G. Jerlov, *Marine Optics* (Elsevier, 1976).
2. J. T. O. Kirk, *Light and Photosynthesis in Aquatic Ecosystems*, 2nd ed. (Cambridge, 1994), pp. 64–70.
3. J. Marra, C. Langdon, and C. A. Knudson, “Primary production, water column changes, and the demise of a *phaeocystis* bloom at the marine light-mixed layers site (59°N, 21°W) in the northeast Atlantic Ocean,” *J. Geophys. Res.* **100**(C4), 6633–6644 (1995).
4. C. R. McClain, K. Arrigo, K. S. Tai, and D. Turk, “Observations and simulations of physical and biological processes at ocean weather station P, 1951–1980,” *J. Geophys. Res.* **101**(C2), 3697–3713 (1996).
5. G. C. Chang and T. D. Dickey, “Coastal ocean optical influences on solar transmission and radiant heating rate,” *J. Geophys. Res.* **109**, C01020 (2004), doi:10.1029/2003JC001821.
6. M. R. Lewis, M.-E. Carr, G. C. Feldman, W. Esaias, and C. McLaren, “Influence of penetrating solar radiation on the heat budget of the equatorial Pacific Ocean,” *Nature* **347**(6293), 543–545 (1990).

7. A. Morel and D. Antoine, "Heating rate within the upper ocean in relation to its bio-optical state," *J. Phys. Oceanogr.* **24**(7), 1652–1665 (1994).
8. Z. P. Lee, K. P. Du, and R. Arnone, "A model for diffuse attenuation coefficient of downwelling irradiance," *J. Geophys. Res.* **110**, C02016 (2005), doi:10.1029/2004JC002275.
9. Z. Lee, C. Hu, S. Shang, K. Du, M. Lewis, R. Arnone, and R. Brewin, "Penetration of UV-visible solar radiation in the global oceans: Insights from ocean color remote sensing," *J. Geophys. Res.* **118**, 1–15 (2013), doi:10.1002/jgrc.20308.
10. T. Surya Prakash and P. Shanmugam, "A robust algorithm to determine diffuse attenuation coefficient of downwelling irradiance from satellite data in coastal oceanic waters," *IEEE J. Sel. Top. Appl. Earth Obs. Remote Sens.*, in press.
11. J. T. O. Kirk, "The vertical attenuation of irradiance as a function of the optical properties of the water," *Limnol. Oceanogr.* **48**(1), 9–17 (2003).
12. J. H. Nielsen and E. Aas, "Relation between solar elevation and the vertical attenuation coefficient of irradiance in Oslofjord," *Univ. of Oslo Rep.* 31 (Univ. of Oslo, 1977).
13. K. S. Baker and R. C. Smith, "Quasi-inherent characteristics of the diffuse attenuation coefficient for irradiance," *Proc. SPIE* **208**, 60–63 (1980).
14. X. Zheng, T. Dickey, and G. Chang, "Variability of the downwelling diffuse attenuation coefficient with consideration of inelastic scattering," *Appl. Opt.* **41**(30), 6477–6488 (2002).
15. H. R. Gordon, "Can the Lambert-Beer law be applied to the diffuse attenuation coefficient of ocean water?" *Limnol. Oceanogr.* **34**(8), 1389–1409 (1989).
16. C. D. Mobley, *Light and Water: Radiative Transfer in Natural Waters* (Academic, 1994).
17. X. Pan and R. C. Zimmerman, "Modeling the vertical distributions of downwelling plane irradiance and diffuse attenuation coefficient in optically deep waters," *J. Geophys. Res.* **115**, C08016 (2010), doi:10.1029/2009JC006039.
18. J. T. O. Kirk, "Volume scattering function, average cosines, and the underwater light field," *Limnol. Oceanogr.* **36**(3), 455–467 (1991), doi:10.4319/lo.1991.36.3.0455.
19. A. Morel and B. Gentili, "Diffuse reflectance of oceanic waters. II Bidirectional aspects," *Appl. Opt.* **32**(33), 6864–6879 (1993), doi:10.1364/AO.32.006864.
20. C. C. Liu, K. L. Carder, R. L. Miller, and J. E. Ivey, "Fast and accurate model of underwater scalar irradiance," *Appl. Opt.* **41**(24), 4962–4974 (2002), doi:10.1364/AO.41.004962.
21. V. B. Sundarabalan, P. Shanmugam, and S. S. Manjusha, "Radiative transfer modeling of upwelling light field in coastal waters," *J. Quant. Spectrosc. Radiat. Transfer* **121**, 30–44 (2013).
22. W. S. Pegau and J. R. V. Zaneveld, "Temperature dependent absorption of water in the red and near infrared portions of the spectrum," *Limnol. Oceanogr.* **38**(1), 188–192 (1993).
23. W. S. Pegau, D. Gray, and J. R. V. Zaneveld, "Absorption and attenuation of visible and near-infrared light in water: Dependence on temperature and salinity," *Appl. Opt.* **36**(24), 6035–6046 (1997).
24. J. R. V. Zaneveld, J. C. Kitchen, and C. Moore, "The scattering error correction of reflecting-tube absorption meters," *Proc. SPIE* **2258**, 44–55 (1994).
25. T. Ohde and H. Siegel, "Derivation of immersion factors for the hyperspectral TriOS radiance sensor," *J. Opt. A, Pure Appl. Opt.* **5**(3), L12–L14 (2003).
26. R. W. Austin and T. Petzold, "The determination of the diffuse attenuation coefficient of sea water using the Coastal Zone Color Scanner," in *Oceanography from Space*, J. F. R. Gower, ed. (Plenum, 1980), pp. 239–256.
27. J. L. Mueller and C. C. Trees, "Revised SeaWiFS prelaunch algorithm for diffuse attenuation coefficient K(490)," in *Case Studies for SeaWiFS Calibration and Validation, Part 4, NASA/TM-1997-104566*, S. B. Hooker and E. R. Firestone, eds. (2003), 41, pp. 18–21.
28. H. R. Gordon, O. B. Brown, and M. M. Jacobs, "Computed relationships between the inherent and apparent optical properties of a flat homogeneous ocean," *Appl. Opt.* **14**(2), 417–427 (1975).
29. J. R. V. Zaneveld, "An asymptotic closure theory for irradiance in the sea and its inversion to obtain the inherent optical properties," *Limnol. Oceanogr.* **34**(8), 1442–1452 (1989), doi:10.4319/lo.1989.34.8.1442.
30. J. T. O. Kirk, "Dependence of relationship between inherent and apparent optical properties of water on solar altitude," *Limnol. Oceanogr.* **29**(2), 350–356 (1984).
31. A. Morel and H. Loisel, "Apparent optical properties of oceanic water: Dependence on the molecular scattering contribution," *Appl. Opt.* **37**(21), 4765–4776 (1998).
32. R. C. Smith and K. S. Baker, "Optical properties of the clearest natural waters (200–800 nm)," *Appl. Opt.* **20**(2), 177–184 (1981).
33. S. Sathyendranath and T. Platt, "The spectral irradiance field at the surface and in the interior of the ocean: A model for applications in oceanography and remote sensing," *J. Geophys. Res.* **93**(C8), 9270–9280 (1988).
34. S. Sathyendranath, T. Platt, C. M. Caverhill, R. E. Warnock, and M. R. Lewis, "Remote sensing of oceanic primary production: Computations using a spectral model," *Deep Sea Res. Part II Top. Stud. Oceanogr.* **36**, 431–453 (1989).
35. Z. P. Lee, K. L. Carder, C. D. Mobley, R. G. Steward, and J. S. Patch, "Hyperspectral remote sensing for shallow waters. I. A semianalytical model," *Appl. Opt.* **37**(27), 6329–6338 (1998).
36. R. H. Stavn and A. D. Weidemann, "Shape factors, two-flow models, and the problem of irradiance inversion in estimating optical parameters," *Limnol. Oceanogr.* **34**(8), 1426–1441 (1989).
37. C. L. Gallegos, D. L. Correll, R. H. Stavn, and A. D. Weidemann, "Modeling spectral diffuse attenuation, absorption, and scattering coefficients in a turbid estuary," *Limnol. Oceanogr.* **35**(7), 1486–1502 (1990).
38. J. Berwald, D. Stramski, C. D. Mobley, and D. A. Kiefer, "Effect of Raman scattering on the average cosine and diffuse attenuation coefficient of irradiance in the ocean," *Limnol. Oceanogr.* **43**(4), 564–576 (1998).

39. A. Herlevi, "A study of scattering, backscattering and a hyperspectral reflectance model for boreal water," *Geophysica* **38**(1–2), 113–132 (2002).
40. M. Wang, S. Son, and W. Shi, "Evaluation of MODIS SWIR and NIR-SWIR atmospheric correction algorithm using SeaBASS data," *Remote Sens. Environ.* **113**(3), 635–644 (2009), doi:10.1016/j.rse.2008.11.005.
41. Y.-H. Ahn and P. Shanmugam, "Derivation and analysis of the fluorescence algorithms to estimate phytoplankton pigment concentrations in optically complex coastal waters," *J. Opt. A Pure Appl. Opt.* **9**, 352–362 (2007).
42. R. H. Stavn, "Effects of Raman scattering across the visible spectrum in clear ocean water: A Monte Carlo study," *Appl. Opt.* **32**(33), 6853–6863 (1993).
43. D. P. Hader, H. D. Kumar, R. C. Smith, and R. C. Worrest, "Effects of solar UV radiation on aquatic ecosystems and interactions with climate change," *Photochem. Photobiol. Sci.* **6**(3), 267–285 (2007).
44. K. Gao, E. W. Helbling, D. P. Hader, and D. A. Hutchins, "Responses of marine primary producers to interactions between ocean acidification, solar radiation, and warming," *Mar. Ecol. Prog. Ser.* **470**, 167–189 (2012).
45. M. A. Moran and R. G. Zepp, "Role of photoreactions in the formation of biologically labile compounds from dissolved organic matter," *Limnol. Oceanogr.* **42**(6), 1307–1316 (1997).
46. P. Shanmugam, V. B. Sundarabalan, Y. H. Ahn, and J. H. Ryu, "A new inversion model to retrieve the particulate backscattering in coastal/ocean waters," *IEEE Trans. Geosci. Remote Sens.* **49**(6), 2463–2475 (2011).
47. A. Vasilkov, N. Krotkov, J. Herman, C. McClain, K. Arrigo, and W. Robinson, "Global mapping of underwater UV irradiances and DNA-weighted exposures using Total Ozone Mapping Spectrometer and Sea-viewing Wide Field-of-view Sensor data products," *J. Geophys. Res.* **106**, 27,205–27,219 (2001).
48. C. R. McClain, G. C. Feldman, and S. B. Hooker, "An overview of the SeaWiFS project and strategies for producing a climate research quality global ocean bio-optical time series," *Deep Sea Res. Part II Top. Stud. Oceanogr.* **51**(1–3), 5–42 (2004), doi:10.1016/j.dsrr.2003.11.001.
49. W. E. Esaias, M. R. Abbott, I. Barton, O. B. Brown, J. W. Campbell, K. L. Carder, D. K. Clark, R. H. Evans, F. E. Hoge, H. R. Gordon, W. M. Balch, R. Letelier, and P. J. Minnett, "An overview of MODIS capabilities for ocean science observations," *IEEE Trans. Geosci. Rem. Sens.* **36**(4), 1250–1265 (1998), doi:10.1109/36.701076.
50. J. L. Mueller, "SeaWiFS algorithm for the diffuse attenuation coefficient, K(490), using water-leaving radiances at 490 and 555 nm, in SeaWiFS Postlaunch Calibration and Validation Analyses," in *SeaWiFS Post Launch Technical Report Series, Part 3, Report 11*, S. B. Hooker and E. R. Firestone, eds. (2002), pp. 24–27.
51. A. Morel, "Optical modeling of the upper ocean in relation to its biogenous matter content (case 1 waters)," *J. Geophys. Res.* **93**(C9), 10,749–10,768 (1988), doi:10.1029/JC093iC09p10749.
52. A. Morel, Y. Huot, B. Gentili, P. J. Werdell, S. B. Hooker, and B. A. Franz, "Examining the consistency of products derived from various ocean color sensors in open ocean (Case 1) waters in the perspective of a multi-sensor approach," *Remote Sens. Environ.* **111**(1), 69–88 (2007), doi:10.1016/j.rse.2007.03.012.
53. S. R. Signorini, S. B. Hooker, and C. R. McClain, "Bio-optical and geochemical properties of the south Atlantic subtropical gyre," *NASA/TM-2003-212253* (2003), pp. 1–43.
54. J. J. Simpson and T. D. Dickey, "The relationship between downward irradiance and upper Ocean structure," *J. Phys. Oceanogr.* **11**(3), 309–323 (1981).
55. Z. P. Lee, K. L. Carder, and R. A. Arnone, "Deriving inherent optical properties from water color: A multiband quasi-analytical algorithm for optically deep waters," *Appl. Opt.* **41**(27), 5755–5772 (2002).
56. T. T. Bannister, "Model of the mean cosine of underwater radiance and estimation of underwater scalar irradiance," *Limnol. Oceanogr.* **37**(4), 773–780 (1992).
57. J. Berwald, D. Stramski, C. D. Mobley, and D. A. Kiefer, "Influences of absorption and scattering on vertical changes in the average cosine of the underwater light field," *Limnol. Oceanogr.* **40**(8), 1347–1357 (1995).
58. N. J. McCormick, "Mathematical models for the mean cosine of irradiance and the diffuse attenuation coefficient," *Limnol. Oceanogr.* **40**(5), 1013–1018 (1995).
59. M. R. Lewis, M.-E. Carr, G. C. Feldman, W. Esaias, and C. McClain, "Influence of penetrating solar radiation on the heat budget of the equatorial Pacific Ocean," *Nature* **347**(6293), 543–545 (1990).
60. J. C. Ohlmann, D. A. Siegel, and C. Gautier, "Ocean mixed layer radiant heating and solar penetration: A global analysis," *J. Clim.* **9**(10), 2265–2280 (1996).
61. T. Platt, S. Sathyendranath, C. M. Caverhill, and M. Lewis, "Ocean primary production and available light: Further algorithms for remote sensing," *Deep Sea Res.* **35**(6), 855–879 (1988).

1. Introduction

Diffuse attenuation coefficient of downwelling irradiance K_d is an important optical property often used in determination of turbidity and classification water types [1, 2], photosynthetic and biological processes in the water column [3, 4] and heat transfer in the upper ocean [5–7]. It is a very useful quantity for many optical analyses of ocean water because of the relative ease in measuring downwelling irradiance E_d and the possibility of measuring K_d remotely [8–10]. It is defined as

$$K_d = \left[\frac{-1}{E_d} \frac{dE_d}{dz} \right]. \quad (1)$$

where E_d ($\text{W m}^{-2} \text{ nm}^{-1}$) is planar downwelling irradiance and z (m) is depth positive downward from the sea surface. The value of K_d at any depth (z) depends not only on the absorption and scattering properties (i.e., Inherent Optical Properties IOPs) of the waters, but also on the angular distribution of the light field at that depth. Even in well-mixed turbid coastal water, where the IOPs are the same, the angular distribution of the light field varies with depth, typically becoming more diffusive with depth as the radiant flux becomes progressively more highly scattered [11]. Thus, K_d has been realized as a descriptor of the underwater light field variation with depth, solar altitude, and time [12, 13].

K_d is an apparent optical property (AOP) that depends on both the medium and geometric structure of the ambient light field. However, as shown in many observations, it is often insensitive to environmental effects except for extreme conditions; therefore it is often regarded as a quasi-inherent optical property depending strongly on changes in IOPs of the water body [14]. This benign behavior of K_d was exploited by Jerlov [1] to develop a classification scheme for oceanic waters. An approximate formula was devised to describe the relationship between K_d and IOPs.

$$K_d = \left[\frac{a + b_b}{\cos(\theta_{sw})} \right]. \quad (2)$$

where a and b_b are the absorption and backscattering coefficients of water respectively, and θ_{sw} is the solar angle measured within the water [15].

Though K_d is a relatively simple quantity to measure *in situ*, its relationship to a , scattering coefficient b , and backscattering b_b is more complicated because K_d is also influenced by the angular structure of the underwater light field and IOPs of the water column [2, 16, 17]. The simplest form, provided by Gordon [15], though valid only for the limited sky and clear oceanic conditions, is given below,

$$K_d = 1.0395 \frac{a + b_b}{\mu_w}. \quad (3)$$

where μ_w is the average cosine of the incident angle of direct solar beam just below the surface (θ_w) after accounting for refraction from the solar zenith angle (θ_s) by Snell's Law $\sin(\theta_w) = \sin(\theta_s)/1.34$ [2, 16]. Note that this relationship is more applicable for clear oceanic waters only, where IOPs are small and vertically homogenous. In turbid coastal waters, scattering typically causes K_d to increase asymptotically and this behavior needs to be accounted for in the model. To understand the nature of K_d , efforts have been made to link K_d with water's IOPs through Monte Carlo simulations [2, 18] leading to a more complicated form of equation [Eq. (4)],

$$K_d = \frac{(\alpha^2 + Gab)^{1/2}}{\mu_w}. \quad (4)$$

where G is a parameter that is related to μ_w and shape of the scattering phase function (or VSF) of the water column [18]. VSF is a property that is seldom measured in the field and cannot be analytically derived especially for turbid waters. Thus, constraining the latter term is more complicated as to make G extremely difficult to parameterize, particularly when the sun is not directly over-head [17]. Thus, Kirk's approximations of G in calculating the average K_d from the surface to the depth (z_1-z_2) are not applicable for turbid coastal waters.

Later, Mobley [16] developed a two flow model providing a simple relationship between K_d and the IOPs,

$$K_d = \frac{a + b_b}{\mu_d} - R \frac{b_b}{\mu_u}. \quad (5)$$

where μ_d and μ_u represent the average cosines of downward and upward plane irradiances, respectively, and R is the ratio of upwelling plane irradiance (E_u) to downwelling plane irradiance (E_d). Applying the definition of R and the definition of the average K_d [Eq. (1)], Lee et al. [8] derived a quasi-analytical model based on RTE to estimate K_d as follows,

$$K_d = m_0 a + v b_b. \quad (6)$$

The parameterization of m_0 and v , however, requires the use of a lookup table (LUT) [8, 19, 20], which may not account for all water conditions. Since R is typically small in optically deep water, the second term on the right side of Eq. (5) is often ignored leading to the common expression:

$$K_d \approx \frac{a + b_b}{\mu_d}. \quad (7)$$

Though this relationship offers a potential solution to relate the vertical variation of K_d to the IOPs, a method to estimate μ_d is not well established for turbid waters.

More recently, Pan and Zimmerman [17] developed a model based on the Hydrolight numerical RT simulations to estimate K_d . The calculations were verified with Hydrolight simulations and validated against *in situ* observations from clear oceanic waters. In order to run the Hydrolight model, one must define the boundary conditions at the surface, the IOPs (i.e., absorption, scattering and scattering phase function) of the water body, and bottom boundary conditions. However, a recent study by Sundarabalan et al. [21] found that such numerical simulations based on the Hydrolight simulations introduce large errors in the underwater light fields for turbid coastal waters, because of the assumption of constant phase function along the depth and simplified boundary conditions (flat surface and bottom). However, it should be noted that the use of homogeneous water and level sea surfaces are not a limitation of Hydrolight itself, which can handle depth-dependent IOPs and wind-blown sea surfaces as well. To overcome some of the above problems, it is necessary to develop a new model to obtain approximately realistic values of the vertical spectral diffuse attenuation coefficient in turbid coastal waters for varying solar zenith angles and in-water optical conditions.

In this study, a new model is developed as a function of angular distribution of incident light and water's absorption and backscattering coefficients along the depth in relatively clear and turbid waters. The model performance is verified with time series *in situ* data as well as the *in situ* data obtained at discrete stations off Point Calimere and Chennai, southeast part of India. These *in situ* data were collected for different solar zenith angles, sky and water conditions before and during the southwest monsoon. To further demonstrate the efficiency of the new model, its results are also compared with those of the existing models.

2. Data and methods

2.1 *In situ* data

Several optical parameters were measured in relatively clear and highly turbid waters off Point Calimere and Chennai (13° 08.534 N; 80° 21.009 E) before and during the southwest monsoon (13–21 May 2012, 15–18 August 2012, and 31 August 2013). Figure 1(a) shows the location map and sampling stations off Point Calimere; this region is shallow (maximum depth 18m) and always dominated by high levels of suspended sediments (resulting from bottom resuspension) caused by tides, alongshore currents and winds [see Figs. 1(c)–1(e)]. In contrast, seawaters off Chennai are relatively clear with very low turbidity [Fig. 1(b)]. The time-series and discrete measurements of various IOPs and AOPs made from several stations around these regions were used to evaluate the performance of the model for predicting the vertical, spatial and temporal variability of K_d for different wavelengths, solar zenith angles and in-water optical conditions. The environmental/ other parameters such as the surface

wind speed, cloud condition, and water depth were recorded for each station where the *in situ* profiling measurements were obtained (Tables 1 and 2).

2.2 Measurement of inherent optical properties

The *In situ* profiles (vertical) of the inherent optical properties were obtained by several sensors (procured from the WETLAB Inc.), namely AC-S, BB9, FLNTU, and CTD (DH4 used for data collection). These sensors mounted on an underwater frame were lowered with help of a winch system in the ship and a single cable was used for transmitting power to the instruments and data to a rugged laptop computer on the deck. The AC-S instrument was used to measure the absorption coefficient ' a ' and the beam attenuation coefficient ' c ' in the entire visible wavelengths (400 to 700). Temperature [22] and salinity corrections [23] were applied to measured absorption and attenuation coefficients, and then scattering correction [24] was applied to the salinity-temperature corrected absorption data. As a result, $(a_t - a_w)$ and $(c_t - c_w)$ were obtained. Here, t and w denote the total and pure water components of the absorption and attenuation coefficients. Pure water coefficients of absorption and attenuation were added to the resultant data in order to obtain the total absorption ' a_t ' and total attenuation ' c_t ' coefficients. The total scattering ' b ' was obtained by subtracting the total attenuation and absorption coefficients. The BB9 sensor was used to measure backscattering ' b_b ' at nine wavelengths 412, 440, 488, 510, 532, 595, 650, 676 and 715. The FLNTU sensors were used to measure chlorophyll and turbidity, while the SBE SeaBird CTD sensors were used to obtain the conductivity-temperature-depth profile data.

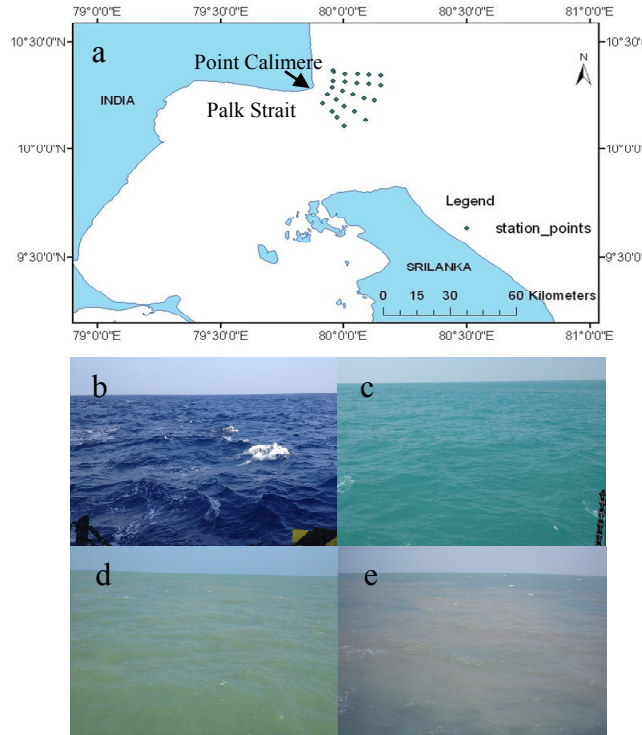


Fig. 1. (a) Location map with sampling stations in coastal waters off Point Calimere on the southeast part of India. *In situ* measurements were made before and during the southwest monsoon (13–21 May 2012 and 15–18 August 2012 respectively). (b) The nature of waters sampled off Chennai and Point Calimere (c–e). (d–e) Characteristic features of coastal waters at a time series station off Point Calimere.

2.3 Radiometric measurements

Table 1. Details of stations sampled before and during the southwest monsoon (13–23 May 2012 and 15–19 August 2012 respectively). Actual depth ≈ measurements depth + 2m.

Coastal waters off Point Calimere before the southwest monsoon (13–21 May 2012)						
Stations	Date	Time	Latitude	Longitude	Measurement Depth (m)	Wind speed ($m s^{-1}$)
T1S0	20/05/2012	09.00	10°22.02'N	79°57.41'E	06.0	4.3
T1S0	20/05/2012	10.30	10°22.02'N	79°57.41'E	06.0	4.3
T1S0	20/05/2012	12.30	10°22.02'N	79°57.41'E	06.0	7.9
T1S0	20/05/2012	15.30	10°22.02'N	79°57.41'E	07.0	7.2
T3S1	19/05/2012	11.00	10°17.06'N	79°57.31'E	07.0	9.3
T4S1	19/05/2012	12.15	10°18.88'N	79°57.51'E	06.5	9.7
T4S2	19/05/2012	12.55	10°18.55'N	80°00.22'E	10.8	9.7
T1S3	18/05/2012	11.00	10°08.9'N	79°08.9'E	06.0	7.2
Coastal waters off Point Calimere during the southwest monsoon (15–18 August 2012)						
T1S0	18/08/2012	09.00	10°22.035'N	79°57.33'E	08.0	5.1-6.2
T1S0	18/08/2012	10.30	10°22.035'N	79°57.33'E	08.0	6.2-7.71
T1S0	18/08/2012	12.00	10°22.035'N	79°57.33'E	08.0	5.1-6.2
T1S0	18/08/2012	15.00	10°22.035'N	79°57.33'E	07.2	5.1-6.2
T2S3	16/08/2012	10.00	10°11.913'N	80°00.21'E	10.1	3.1-4.1
T2S4	15/08/2012	16.10	10°10.574'N	80°02.67'E	13.0	4.1-5.1
T3S3	16/08/2012	13.35	10°15.240'N	80°02.27'E	13.2	6.2-7.7
T5S2	17/08/2012	13.35	10°20.949'N	80°00.30'E	11.5	13.00
Coastal waters off Chennai during the southwest monsoon (31 August 2013)						
CH1	31/08/2013	12.00	13°08.715'N	80°21.041'E	20	8.00
CH1	31/08/2013	13.30	13°08.715'N	80°21.041'E	19.9	8.00
CH1	31/08/2013	15	13°08.715'N	80°21.041'E	19.8	8.00

Table 2. The range of absorption (a), backscattering (b_b), Chl and Turbidity at various stations off Point Calimere and Chennai before and during the southwest monsoon.

Coastal waters off Point Calimere before the southwest monsoon (13–21 May 2012)				
	$a(490) (m^{-1})$	$b_b (490) (m^{-1})$	Chl ($\mu g L^{-1}$)	Turbidity
T1S0	~0.24-1.18	~0.099-0.248	~0.98-1.19	~9.75-10.43
T1S0	~0.19-1.11	~0.099-0.257	~1.12-1.64	~8.49-12.51
T1S0	~0.13-0.77	~0.091-0.187	~0.96-1.92	~6.06-7.03
T1S0	~0.12-0.65	~0.079-0.253	~1.03-6.58	~5.23-15.23
T3S1	~0.27-1.21	~0.099-0.237	~0.72-1.07	~6.64-8.39
T4S1	~0.25-1.00	~0.014-0.034	~0.81-1.05	~5.96-7.56
T4S2	~0.12-0.66	~0.002-0.005	~0.81-2.70	~0.92-1.26
T1S3	~0.16-0.68	~0.008-0.019	~0.63-0.99	~3.49-7.23
Coastal waters off Point Calimere during the southwest monsoon (15–18 August 2012)				
T1S0	~0.14-0.66	~0.003-0.006	~3.25-7.13	~1.26-1.65
T1S0	~0.15-0.66	~0.002-0.007	~3.49-7.44	~1.26-1.65
T1S0	~0.17-0.76	~0.003-0.007	~3.42-8.29	~1.31-1.94
T1S0	~0.21-0.79	~0.004-0.007	~7.56-12.60	~1.65-2.52
T2S3	~0.17-0.72	~0.002-0.005	~2.72-8.16	~0.68-1.55
T2S4	~0.24-0.91	~0.002-0.003	~3.82-9.30	~0.73-1.36
T3S3	~0.18-0.81	~0.001-0.003	~2.81-8.87	~0.44-1.60
T5S2	~0.16-0.71	~0.002-0.004	~2.82-7.84	~0.68-1.26
Coastal waters off Chennai during the southwest monsoon (31 August 2013)				
CH1	~0.04-0.061	~0.006-0.009	~0.24-2.48	~0.01-0.97
CH1	~0.05-0.052	~0.006-0.007	~0.11-3.69	~0.01-2.91
CH1	~0.07-0.072	~0.006-0.0068	~0.31-0.65	~0.01-0.49

The underwater radiometric profiling measurements were made using three RAMSES (Trios) hyperspectral radiometers; i.e., one ARC and two ACC radiometers used to measure upwelling radiance, upwelling irradiance and downwelling irradiance respectively. The irradiance sensor has a built-in pressure sensor which provides the corresponding depth in the water column. All these radiometric quantities were measured in the visible and near-infrared (350–950 nm) wavelengths with spectral accuracy of 3.3nm. These sensors mounted on an underwater frame were deployed in the same way as the WETLAB sensors. The MSDA_XE software was used to record the radiance and irradiance data and export them from the database to a PC on the deck for further processing. Since the radiance sensor was immersed in water, the immersion factors (wavelength-dependent correction factors) from Ohde et al. [25] were applied to the measured radiance signal (not used in this study). Data from the radiometers and WETLAB sensors were then interpolated to common depth and wavelength for further analysis.

3. Model description

In Eq. (1), $E_d(z)$ needs to be measured within an infinitesimal range of z to know the vertical diffuse attenuation coefficient. It is nearly impossible to accurately determine $K_d(z)$ in the field due to wave introduced fluctuations in the subsurface light field [21]. This obstacle is overcome by calculating the diffuse attenuation coefficient between the irradiances measured over distant depths as described below. The variables z_1 and z_2 are set far apart to ensure reliable measurements of E_d change. *In situ* measurements for K_d determination can be carried out with at least two depth values, and hence the average \bar{K}_d is defined by

$$\bar{K}_d(z_1 \leftrightarrow z_2) = \frac{1}{z_2 - z_1} \ln \left(\frac{E_d(z_1)}{E_d(z_2)} \right). \quad (8)$$

A commonly used and accurate alternative is to calculate the linear regression coefficient of $\ln E_d(z)$ with respect to depth over the depth interval of interest. In fact, an exact expression for depth-averaged K_d over any depth interval from the surface down to depth z can be written as

$$\bar{K}_d(0 \leftrightarrow z) = \frac{\int_0^z K_d(z) dz}{z}. \quad (9)$$

It should be noted that since the accuracy of this \bar{K}_d depends on the value of z used in the measurements, its value is likely to be significantly different from that of the previous \bar{K}_d [Eq. (8)] in the upper layers of the water column where angular distribution of incident light has its effects [11].

In the past decades, many remote sensing and *in situ* methods have been used to determine diffuse attenuation coefficient [9, 18, 26–31]. Efforts have been made to relate K_d with water's IOPs such as the absorption, scattering and backscattering coefficients. Thus, K_d is simplified as [32],

$$K_d(z) = a + b_b. \quad (10)$$

or

$$K_d = \frac{(a + b_b)}{\mu_0}. \quad (11)$$

[33, 34]. As noted earlier, these simple approximations work fairly well for clear oceanic waters but are progressively limited in turbid coastal waters. Thus, it is important to develop a

new model of K_d using a , b_b and θ for estimating its vertical spectral distributions in relatively clear and turbid coastal waters.

Building on the ideas of Gordon [15], Kirk [11, 18], Mobley [16] and Lee et al. [35] gives rise to the development of a new model for calculating the vertical spectral diffuse attenuation coefficient (K_d) (wavelengths 400–700 nm) for the near-surface, intermediate and bottom layers and for various solar zenith angles and sky conditions. Thus, $K_d(\lambda, \theta, z)$ is modeled based on the concept that AOPs of the ocean are determined by the IOPs of seawater and solar zenith angle (θ) through the radiative transfer equation [28]. If the values of a , b_b , θ and sea state conditions are known, $K_d(\lambda, \theta, z)$ values can be calculated by the new model. The model input parameters are derived from *in situ* measurements, wherein preprocessing steps are used to interpolate and categorize these measured data for our analysis. It includes the computation of solar zenith angles and selection of data sets for different depth intervals. The solar zenith angle for each station is calculated based on the recorded information (year, date, time, longitude, and latitude). The average K_d values between depth layers are then calculated as follows,

$$K_d(z \rightarrow z_1) = \frac{1}{(Z_1 - Z)} [\ln E_d(z) - \ln E_d(Z_1)]. \quad (12)$$

where z , z_1 are depths and E_d is the downwelling irradiance just below the surface. The proposed K_d model is derived based on the radiative transfer equation [36] coupled with empirical proportionality constants A_1 , A_2 and A to extend the range of applicability from clear waters to coastal waters [Eq. (13)].

$$K_d = [A(A_1 a + A_2 b_b)] + C_3. \quad (13)$$

$$A = \frac{1}{C_1 C_2}. \quad (14)$$

$$C_1 = 4.848 + 0.01696z - 4.84 \cos(\theta). \quad (15)$$

$$C_2 = 14.98 + 0.3228z - 32.32 \cos(\theta) - 0.3562z \cos(\theta) + 17.65(\cos(\theta))^2. \quad (16)$$

$$C_3 = -13.13 + 0.6286z + 30.62 \cos(\theta) - 0.1292z^2 - 0.2724z \cos(\theta) - 17.14(\cos(\theta))^2. \quad (17)$$

$$A_1 = 1 + \cos(\theta). \quad (18)$$

$$A_2 = \left[a^3 + \left(\frac{b_b}{a} \right)^2 - b_b^2 a - \left(\frac{b_b}{a} \right)^4 \right]. \quad (19)$$

A_1 , A_2 and A are the parameters encompassing the variation of θ and b_b/a and other empirical coefficients C_1 and C_2 and C_3 respectively are defined in Eqs. (14)–(19). The dependency of the newly defined parameters A_1 on θ , and A_2 on b_b/a are shown in Fig. 2 (top panels). A_1 decreases gradually with increasing solar zenith angle, while A_2 shows a steep decrease with increasing values of b_b/a . Dependency of the derived coefficients C_1 , C_2 and C_3 on solar zenith angle and depth are shown in Fig. 2 (bottom panels). C_1 increases with solar zenith angle and also increases linearly with increasing depth, whereas C_2 and C_3 almost remain constant at lower solar zenith angles and show an increasing trend at higher solar zenith angles. C_2 and C_3 decrease with increasing depth. These parameterizations are necessary to take into account some of the complex issues associated with internal sources (i.e., Raman scattering and chlorophyll fluorescence which are difficult to distinguish with radiometric measurements), vertical inhomogeneities and solar incident radiation. Rearranging the above equations [Eqs. (13)–(19)] gives rise to the following model for predicting K_d ,

$$K_d = \left[\left(\frac{1}{C_1 C_2} \right) \right] \left[(1 + \cos(\theta)) a + \left(a^3 + \left(\frac{b_b}{a} \right)^2 - b_b^2 a - \left(\frac{b_b}{a} \right)^4 \right) b_b \right] + C_3. \quad (20)$$

This model is more appropriate to obtain approximately realistic values of the vertical spectral diffuse attenuation coefficient in relatively clear and highly turbid coastal waters [Table 2]. The new model takes into account the vertical inhomogeneities in the absorption and backscattering coefficients which usually pose special problems for detailed modeling of the underwater light fields in turbid coastal waters [37].

4. Model performance assessment

The performance of the new model for deriving the vertical spectral diffuse attenuation coefficient is evaluated using independent *in situ* data from three cruises (13–21 May 2012, 15–18 August 2012, and 31 August 2013 before and during the southwest monsoon) in highly turbid coastal waters off Point Calimere and relatively clear waters off Chennai. Three time series *in situ* data and those obtained at discrete stations are used for evaluation of the new model and existing models. The detailed information of these data sets (e.g., $a(490)$, $b_b(490)$, [Chl] and turbidity) is given in Tables 1 and 2. To gain insights into the model performance, scatter plots of the modeled K_d values versus *in situ* K_d values and errors between these data are examined. Two basic statistical measures used in this study are the root mean square error ($RMSE$) and mean relative error (MRE), which are defined as follows:

$$RMSE = \sqrt{\frac{\sum_{i=1}^N (\log k_d^{model} - \log k_d^{in-situ})^2}{N-2}}. \quad (21)$$

$$MRE = \left[\sum_{i=1}^N \frac{\log k_d^{model} - \log k_d^{in-situ}}{\log k_d^{in-situ}} \right] \times 100. \quad (22)$$

Besides, the accuracy of K_d predictions is also assessed based on the slope (S), intercept (I), bias, and correlation coefficient (R^2) of the linear regression between the *in situ* and modeled K_d values.

5. Results

5.1 In situ IOPs data

The spectral absorption and backscattering coefficients (a and b_b) are the important inherent optical properties often used in the radiative transfer simulations and bio-optical modeling studies to determine the underwater light fields [9, 17, 21, 38]. The magnitude and spectral dependence of these coefficients are not only determined by seawater alone but also by other optically important constituents including phytoplankton, colored dissolved organic matter (CDOM) and non-algal particles. The phytoplankton, non-algal particulates and seawater absorb and scatter light, whereas CDOM is a dominant absorber of light but contributes negligibly to scattering [16].

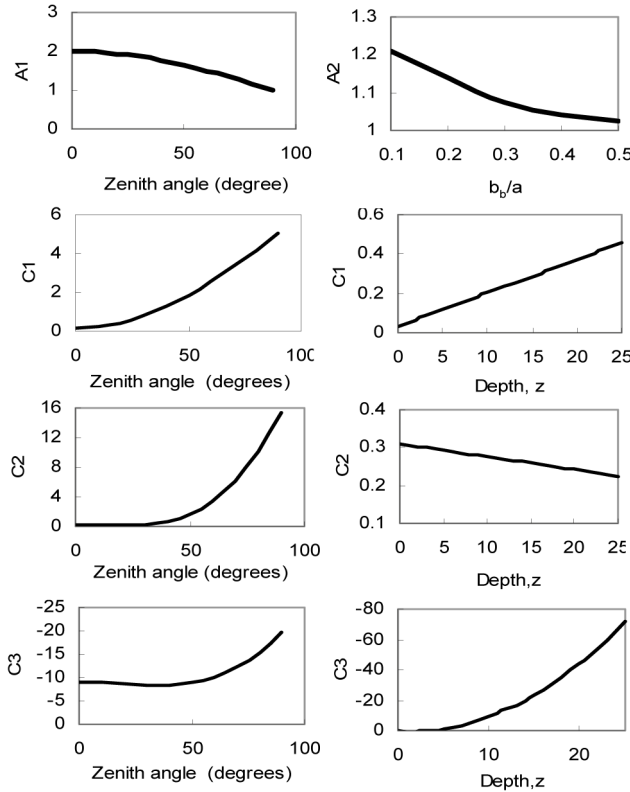


Fig. 2. Dependency of the newly defined parameters A_1 , A_2 , C_1 , C_2 on θ , b_b/a and depth.

5.2 In situ time series IOP profiles along the depth

To demonstrate the performance of the new model and existing models, we use the IOP profile data obtained from a wide range of waters in the coastal ocean as determined by vertical inhomogeneity and stratified conditions. Figure 3 shows the depth-averaged vertical profiles of IOPs (a and b_b) for a time series coastal station off Point Calimere before and during the southwest monsoon (for brevity, these profiles are shown only for some key wavelengths 412, 443, 490, 510 and 551nm). In May 2012, a and b_b values are significantly high at solar zenith angles $-43^\circ \sim 12^\circ$ although showing less variation along the depth. When the solar zenith angle $\sim 51^\circ$, the absorption coefficients are stable from the top layer to the middle layer and decrease slightly with depth at the bottom layer. The backscattering coefficients show a similar trend at the surface and middle layers, but with an abrupt increase at the bottom layer. The high a and b_b values and an increasing trend of b_b could be due to benthic resuspension and advection of the organic and inorganic particulate materials caused by the alongshore currents and tides. The time series measurements of a and b_b during the southwest monsoon (August 2012) show relatively low a values and very low b_b values compared to those of the pre-southwest monsoon. Note that the absorption coefficients are slightly elevated at the surface and bottom layers around -45° and -23° , being reduced noticeably at the intermediate layer. On the other hand, the absorption coefficients decrease with increasing depth at 3° and 42° . The b_b profiles show a slight variation (i.e., a decreasing or increasing trend) at -45° and 42° but are more stable along the depth at -23° and 3° .

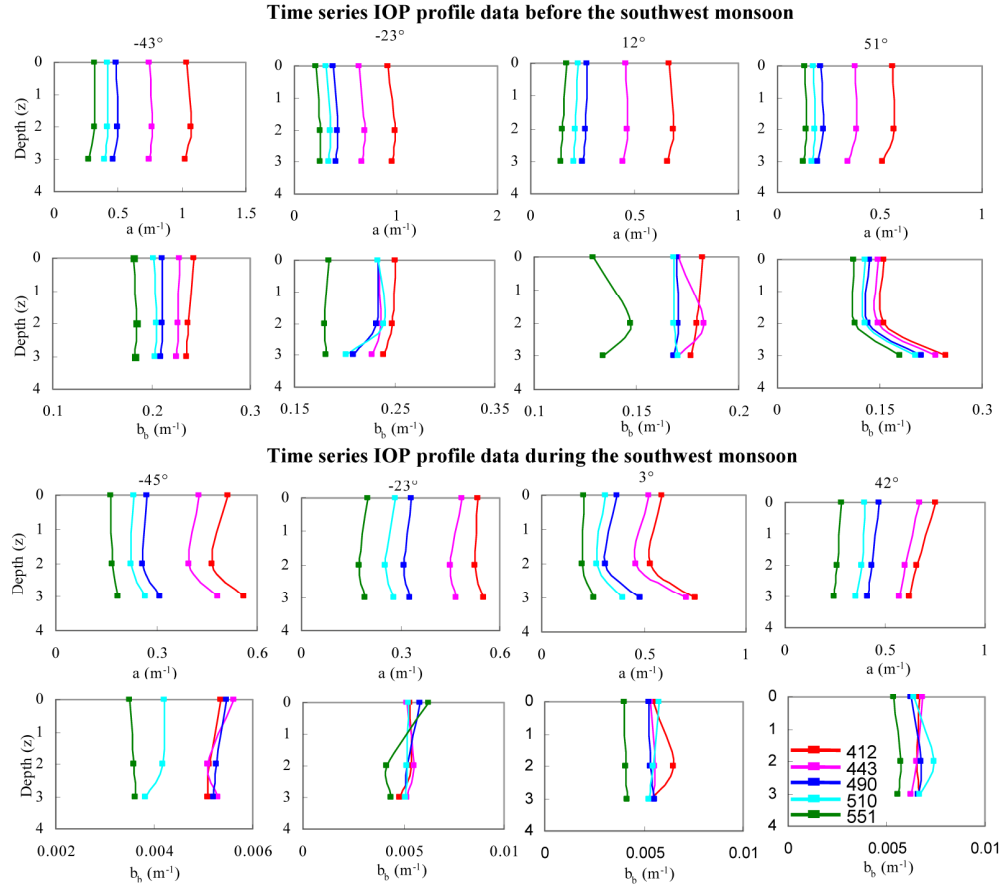


Fig. 3. The depth-averaged vertical profiles of the absorption coefficients (a), backscattering coefficients (b_b) at different wavelengths (412, 443, 490, 510 and 551 nm) measured (time series) during the May 2012 (before southwest monsoon) and August 2012 (during southwest monsoon) cruises in coastal waters off Point Calimere of southern India. Note that the negative sign indicates before noon and the positive sign indicates after noon for describing the solar zenith angle.

The vertical profiles of the depth-averaged IOPs from discrete stations obtained before the southwest monsoon (May 2012), display a and b_b values increasing steadily with depth [Fig. 4] due to advection of the resuspended materials from coastal waters to offshore waters (as captured at these stations). The increase in b_b is due to the increase in the amount of inorganic particles, which scatter light at larger angles than organic particles [39]. During the southwest monsoon, the a and b_b values are reduced although fluctuating slightly along the depth. The b_b values are significantly lower than those observed before the commencement of southwest monsoon, which may be indicative of relatively clear waters encountered at these stations during this period.

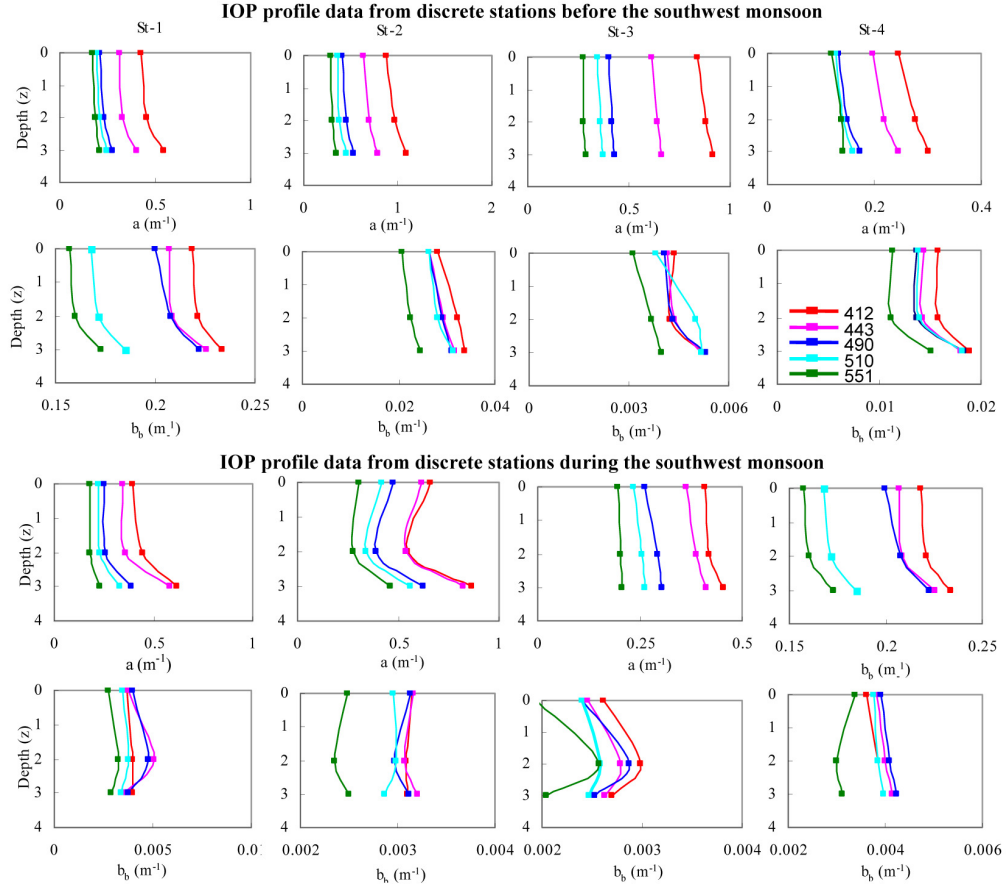


Fig. 4. The depth-averaged vertical profiles of the absorption coefficients (a), backscattering coefficients (b_b) at different wavelengths measured during the May 2012 (before the southwest monsoon) and August 2012 (during the southwest monsoon) cruises in coastal waters off Point Calimere of southern India.

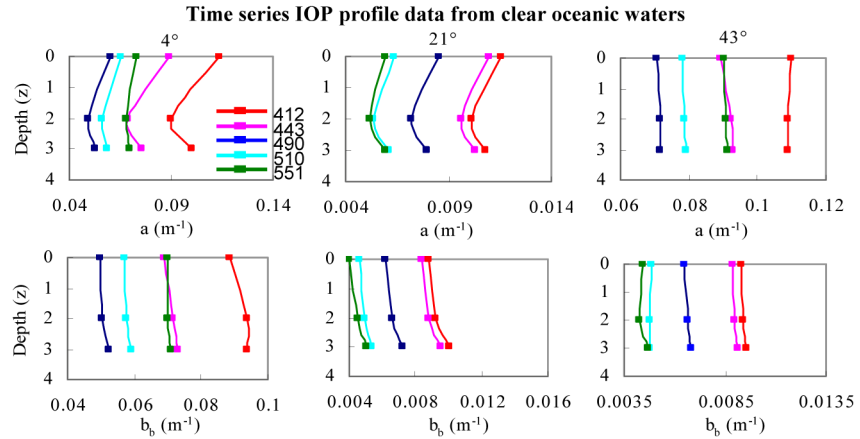


Fig. 5. The depth-averaged vertical profiles of the absorption coefficients (a) and backscattering coefficients (b_b) measured in clear waters of Chennai during August 2013.

For clear oceanic waters off Chennai, both the a and b_b coefficients are inevitably low as compared to those observed in relatively clear and turbid coastal waters [Fig. 5] [Table 2]. These coefficients are mainly dominated by the seawater itself when Chl and turbidity levels are in the range of $0.11\text{--}3.69 \mu\text{g L}^{-1}$ and $0.01\text{--}2.91\text{NTU}$ respectively (slightly high values observed only at the deep layer). Nevertheless, the vertical profiles of these IOPs show significant fluctuations at 4° and 21° or vertically homogenous patterns at 43° . Thus, these IOP profile data can provide a better evaluation of the K_d models for different wavelengths, in-water optical conditions and solar zenith angles.

5.3 Model implementation

The spectra of K_d generated from the new model and existing models were compared with the corresponding data from field measurements collected during three cruises in both clear oceanic waters and highly turbid waters. First, we perform these comparisons for three time-series K_d data (two from highly turbid waters off Point Calimere and one from clear waters off Chennai) for the entire visible wavelengths (400–700nm), three depth layers and different zenith angles [Fig. 6 (where a-c correspond to the surface, intermediate and bottom layers respectively)]. Note that the modeled and *in situ* spectra $K_d(\lambda, z, \theta)$ match very well in both magnitude and spectral shape in coastal waters with a wide range of turbidity conditions off Point Calimere during July and August 2012. Because of high turbidity [see Table 2] encountered before the commencement of southwest monsoon, the values of $K_d(\lambda)$ are increasingly high in the short wavelengths (blue), decreasing steadily from the blue to the green, and then increasing gradually from the green to the NIR wavelengths. The down-slope (from the blue to the green wavelength) is generally steeper than the up-slope (from the red to the NIR wavelengths) for these conditions. The increase in $K_d(\lambda)$ at the blue wavelengths are likely due to the increased attenuation of light by particulate matter (mostly sediments and perhaps dissolved substances) in the water column [40]. There is a slight deviation of the modeled $K_d(\lambda)$ (overestimation in the blue and / or red/NIR wavelengths) in the intermediate and bottom layers at -43° and surface and bottom layers at 12° , which may be caused by the radiometric/photometric measurements including errors associated with the effects of sea surface waves, tides and ship conditions, and by time and space variations in environmental variables. As a result, these deviations are also likely due to the enhanced contribution of resuspended sediments to the backscattering coefficients at this station. Examination of the time-series data of the southwest monsoon from the same station shows good agreement between the modeled $K_d(\lambda)$ and *in situ* $K_d(\lambda)$ for all depth layers and solar zenith conditions [Fig. 6] (bottom panels). During this period, turbidity level is significantly reduced ($0.44\text{--}1.94 \text{ NTU}$) but the chlorophyll level is elevated up to $12.6 \mu\text{g L}^{-1}$ compared to those obtained before the southwest monsoon (thus reduced b_b and nearly the same a values in these moderately turbid waters). Consequently, the diffuse attenuation coefficient is almost equal at the blue and NIR wavelengths, with a pronounced trough at the green wavelengths. This trend of the decreased and increased K_d values in the short wavelengths and NIR wavelengths is attributable to the reduced particle concentrations and increased water content (its absorption thus enhanced the attenuation coefficient at the NIR wavelengths). It is evident that these *in situ* $K_d(\lambda)$ spectra for optically/vertically homogenous and inhomogeneous conditions are well reproduced (often virtually indistinguishable from the measured spectra) by the new model. Application of the other two models (Model 1 [15] and Model 2 [18]) to these time series *in situ* data from highly turbid waters indicates that their $K_d(\lambda)$ spectra are very much biased with large errors across the wavelengths for different depth layers. As a result, significant deviations with respect to the measured $K_d(\lambda)$ spectra are expected with these models.

To see how the models work for different waters, Fig. 7 shows the comparison of modeled K_d versus *in situ* K_d values (for three different depth layers) from four discrete stations covering relatively clear and moderately turbid waters off Point Calimere during July 2012 and August 2012. In relatively clear waters, the $K_d(\lambda)$ values are small at the blue and green wavelengths but increasing towards the longer wavelengths as a result of the increased water absorption (e.g., St-1 and St-4). In moderately turbid waters, the $K_d(\lambda)$ values show a reverse

trend as already reported for highly turbid waters at the time series station. For these stations, the new model $K_d(\lambda)$ values are in remarkable agreement (in spectral shape and magnitude) with the measured $K_d(\lambda)$ values. Small differences are observed at the longer wavelengths (especially at the intermediate and bottom layers at St-1 and surface and bottom layers at St-4), possibly due to the effect of solar zenith angles (for the near-surface layers) and/ or changes in the water column optical conditions.

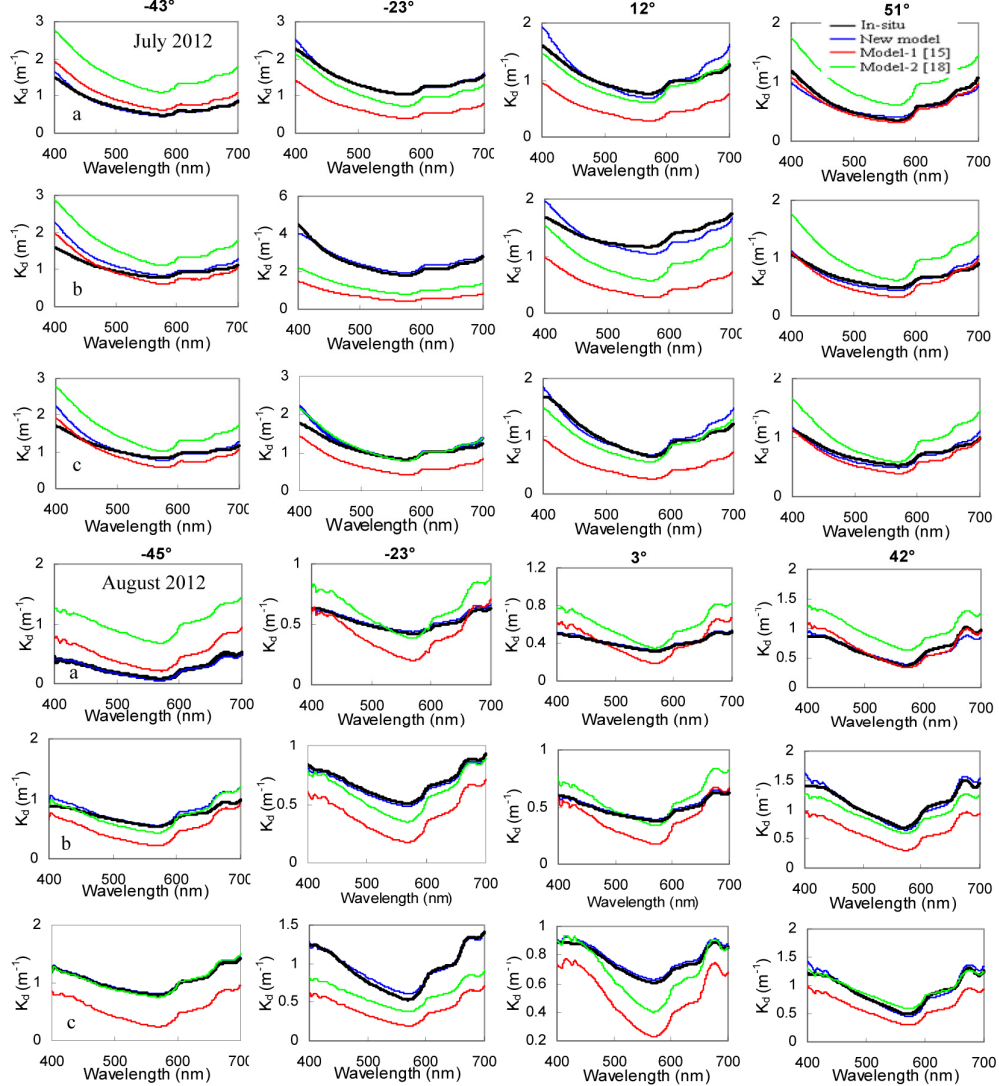


Fig. 6. Comparison of the diffuse attenuation coefficient $K_d(\lambda)$ derived from the new model and existing models for different depth layers (z) at the time series coastal station (relatively clear to turbid waters) off Point Calimere before and during the southwest monsoon (May 2012 and August 2012 respectively). (a) Diffuse attenuation coefficient just below the surface, (b) Diffuse attenuation coefficient at the intermediate layer, (c) Diffuse attenuation coefficient at the bottom layer.

It is important to note that these deviations in modeled $K_d(\lambda)$ values above 600nm for the intermediate and bottom layers may be caused by the existence of internal light sources, the most important of which are Raman scattering and chlorophyll fluorescence whose contributions to K_d variability are found to be minimal in turbid waters [14, 41]. However, the

$K_d(\lambda)$ values produced by the existing models are very much overestimated or underestimated when compared to the measured $K_d(\lambda)$ spectra in relatively clear and moderately turbid waters off Point Calimere. These results (for the times series and discrete stations) suggest the existing models appear to be insensitive to changes in the angular distribution of light reaching the sea surface and water column optical conditions (including vertical/horizontal variations).

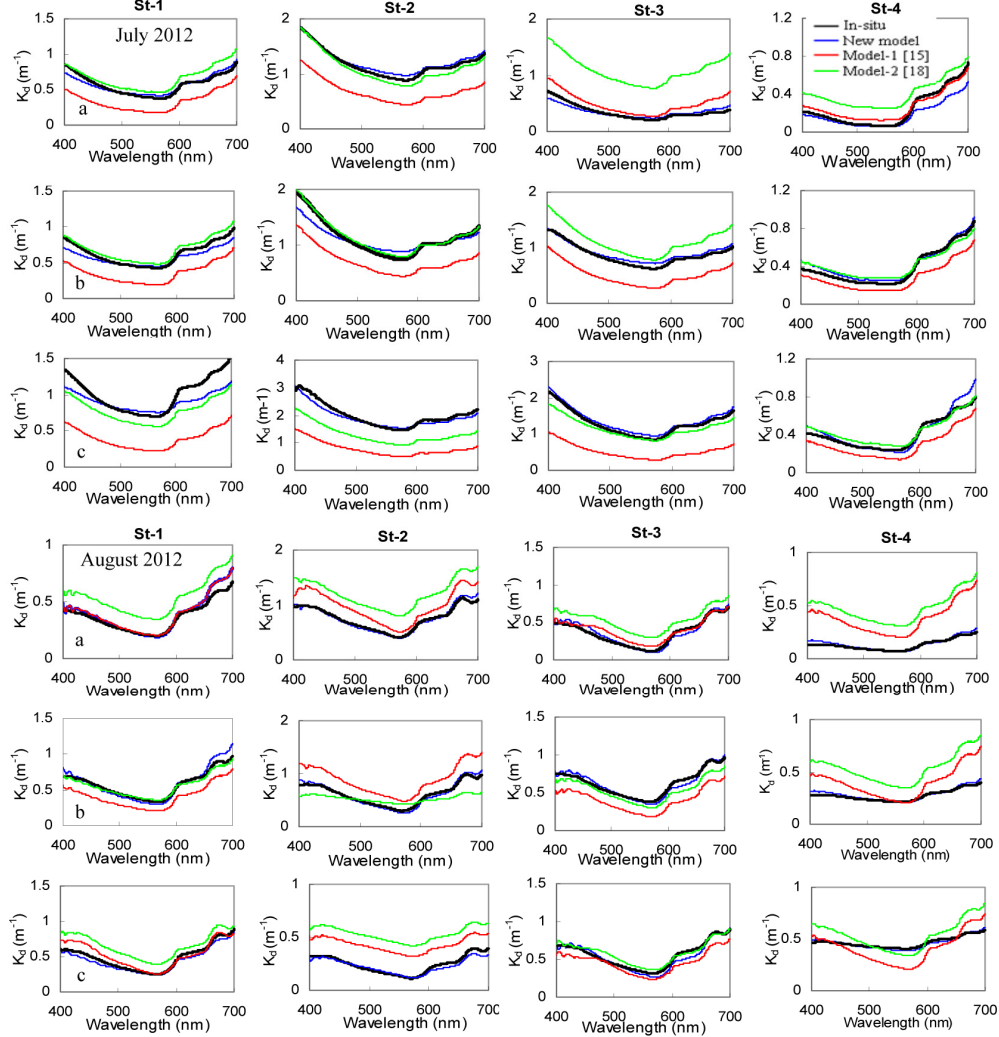


Fig. 7. Comparison of the diffuse attenuation coefficient $K_d(\lambda)$ derived from the new model and existing models for different depth layers (z) at different coastal stations (relatively clear to turbid waters) off Point Calimere before and during the southwest monsoon (May 2012 and August 2012 respectively). (a) Diffuse attenuation coefficient just below the surface, (b) Diffuse attenuation coefficient at the intermediate layer, (c) Diffuse attenuation coefficient at the bottom layer.

The performance of these models is also evaluated using another set of the time series *in situ* data obtained in clear oceanic waters off Chennai on 31 August 2013. These waters are different from the previous cases, exhibiting very low turbidity 0.01-2.91 and chlorophyll 0.11~3.69 $\mu\text{g L}^{-1}$ which significantly reduced both the absorption and backscattering coefficients. Figure 8 shows the comparison of modeled $K_d(\lambda, z, \theta)$ and *in situ* $K_d(\lambda, z, \theta)$ for this time series data set (for limited coverage). These plots depict an increasing dependence of K_d

on the solar zenith angle and its resonance structure is typical of the absorption by water molecules from the blue to the red wavelengths [15, 18].

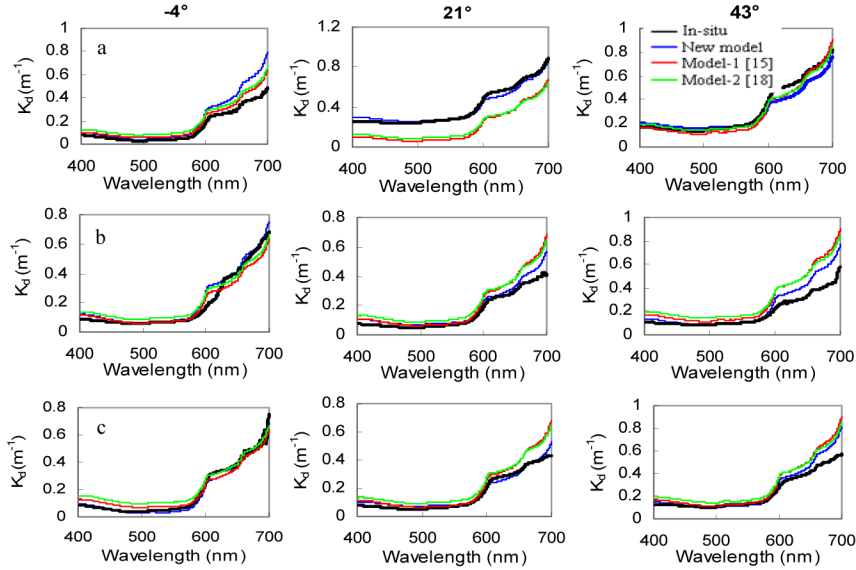


Fig. 8. Comparison of the diffuse attenuation coefficient $K_d(\lambda)$ derived from the new model and existing models for different depth layers (z) at the time series station off Chennai (Clear waters) during the southwest monsoon (31 August 2013). (a) Diffuse attenuation coefficient just below the surface, (b) Diffuse attenuation coefficient at the intermediate layer, (c) Diffuse attenuation coefficient at the bottom layer.

Physically, K_d corresponds to the attenuation of irradiance and is proportional to the path length of photon in water. For pure water, K_d is expected to be inversely proportional to μ [14, 18]. However, in naturally occurring water bodies, scattering is caused by water molecules and suspended particulate matters which cause the underwater light field to become more isotropic and its dependence on illumination geometry is limited. Thus, the correlation between K_d and incident solar zenith angle is less significant within the short wavelength domain ($\lambda < 570$ nm) [Fig. 8]. It also shows that the K_d values are distinctly low at $\lambda < 570$ nm and remarkably high in the longer wavelengths ($\lambda > 570$ nm). An increasing trend in K_d values is due to the absorption effect of seawater. The solar zenith angle has a profound effect on K_d at $\lambda > 600$ nm, although this correlation between K_d and solar zenith angle diminishes with increasing depth due to more isotropic light field at greater depth. Monte Carlo simulations in such clear oceanic waters showed that Raman scattering produces strong vertical gradients in the average cosine and the diffuse attenuation coefficient of irradiance, especially at longer wavelengths and for low chlorophyll waters [42]. Since many of these varying factors are taken into account with the newly defined calibration coefficients, the new model produces more accurate $K_d(\lambda, z, \theta)$ values than those of the existing models for different wavelengths, solar zenith angles and in-water optical conditions [Fig. 8].

To further illustrate the differences between model and *in situ* K_d values over a range of solar zenith angles, these two data sets (only for some key wavelengths) are plotted as a function of solar zenith angles for the time series measurements in coastal waters off Point Calimere (before and during the southwest monsoon, May 2012 and August 2012 respectively) [Fig. 9]. These plots not only show good agreement between modeled (new model) and *in situ* K_d values but also depict their variation for different solar zenith angles and varying in-water optical conditions. Angular dependencies of K_d at seven wavelengths are clearly evident in these plots; i.e., the K_d values are consistently high in the upper layers (May 2012) for medium and high solar positions (e.g., $\theta = -30\text{--}0^\circ$), while these features are suppressed or becoming independent of solar zenith angles at the bottom layers. These high

K_d values apparently coincide with high levels of suspended sediments that were seen advected by the alongshore currents and tidal waters in May 2012 [see Figs. 1(d) and 1(e)]. This means that K_d tends to be less dependent on the solar zenith angles owing to the increasing of scattering effects of these suspended particulate (inorganic) materials in the water column (dominated by the advection process). To our knowledge, this is the first time to show the dependency of K_d on solar zenith angles and in-water (highly turbid) optical conditions with experiments and modeling results.

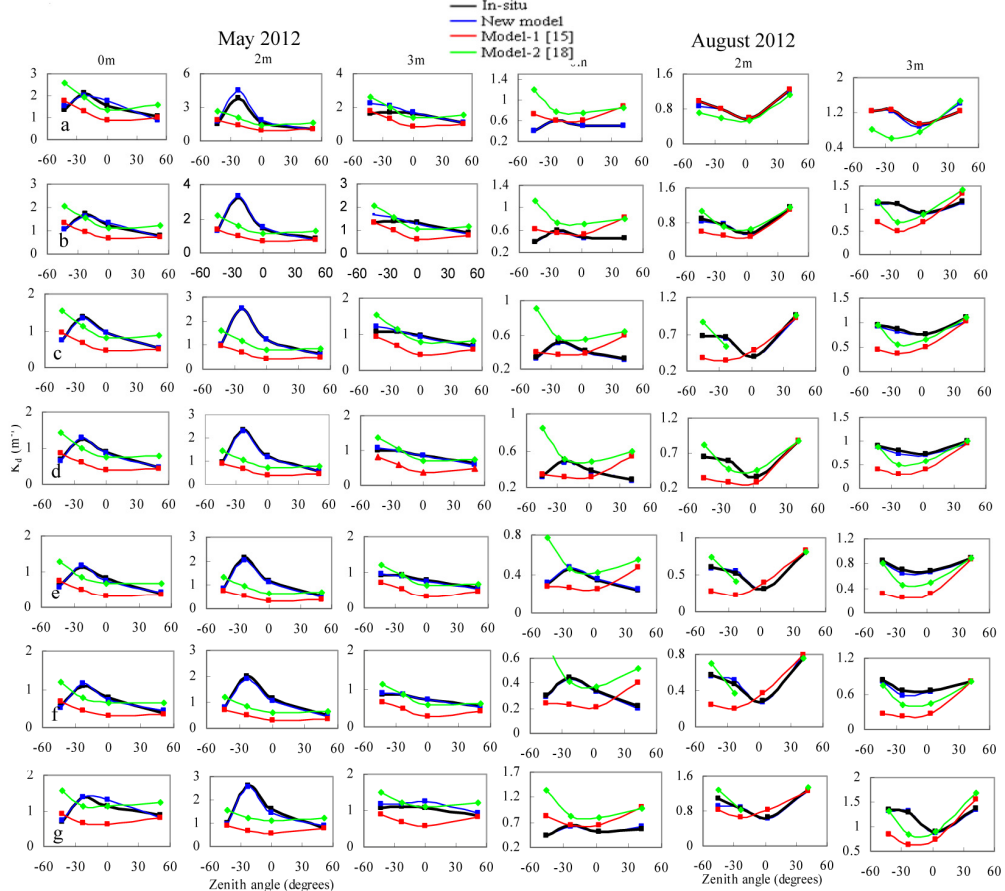


Fig. 9. Comparison of the modeled $K_d(\lambda)$ with *in situ* $K_d(\lambda)$ for different zenith angles at the time series coastal station off Point Calimere before and during the southwest monsoon: Key wavelengths a) 412nm, b) 443nm, c) 490nm, d) 510nm, e) 531nm, f) 551nm, and g) 670nm. (0, 2 and 3m correspond to different depth layers (z)).

On the other hand, the new model reproduces measured K_d for relatively clear and moderately turbid waters sampled during August 2012. Note that the K_d values show similar angular patterns in the near-surface layer but are reversed in the intermediate and bottom layers, thus not following the simple $K_d \propto 1/\mu$ relationship. K_d tends to become low (with increasing wavelengths $\lambda < 555\text{nm}$) at the intermediate and bottom layers when the solar zenith angle is within -30° – 30° , which may be caused by the prevailing low particle conditions during these time periods. However, the $K_d(670)$ values are slightly elevated at the intermediate and bottom layers likely due to the presence of more detrital/inorganic particles. These variations in K_d for different solar and in-water optical conditions confirm the previous hypothesis that this property is a quasi-continuous function of the solar zenith angle and water's IOPs in relatively clear and moderately turbid oceanic waters [14]. Unfortunately,

other two models are unable to provide accurate K_d values that exhibit nearly same patterns (variations) regardless of the solar zenith angles and in-water optical conditions.

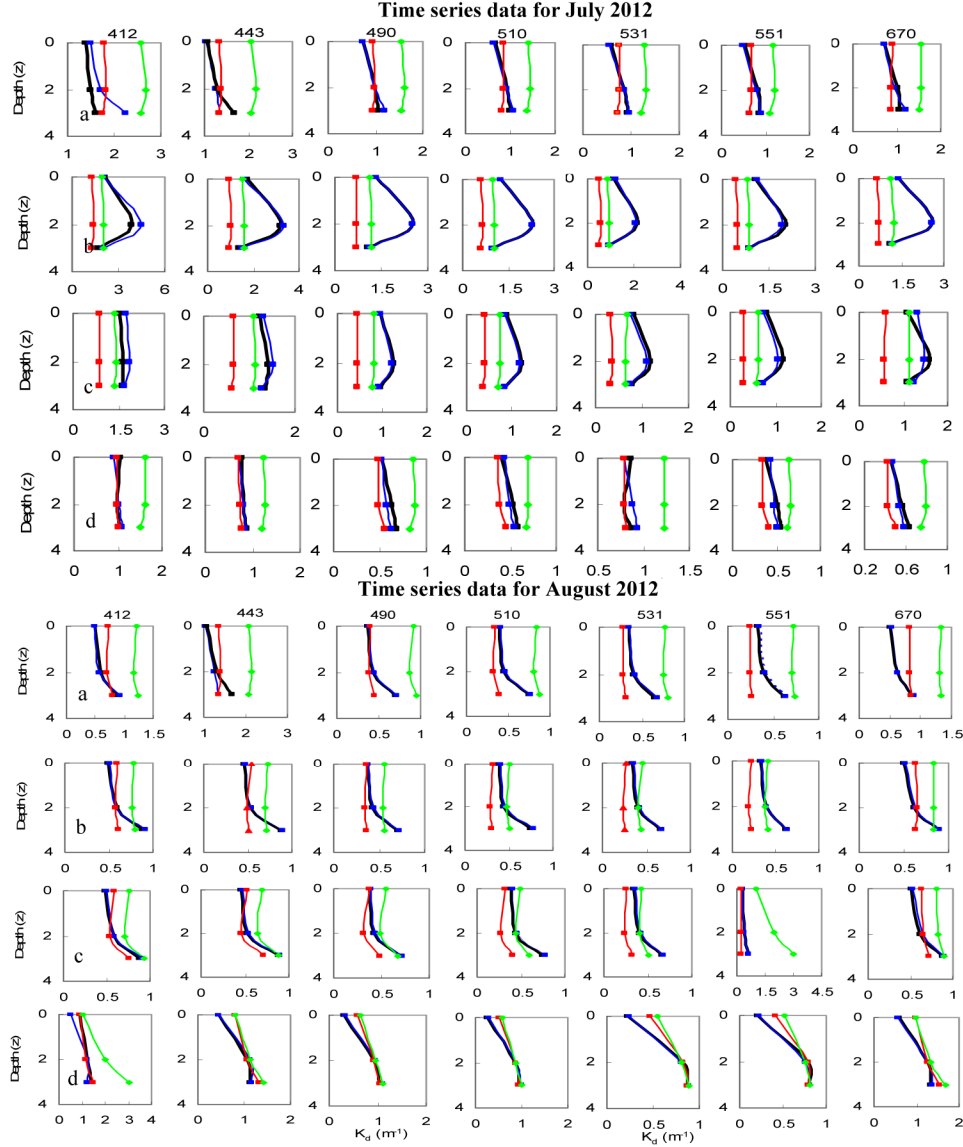


Fig. 10. Comparison of the modeled $K_d(\lambda)$ with *in situ* $K_d(\lambda)$ for different depth layers (z) at the time series coastal station off Point Calimere before and during the southwest monsoon (May 2012 and August 2012). (a-d) Time series measurements at $-43^\circ, -23^\circ, 12^\circ, 51^\circ$ in May 2012, and $-45^\circ, -23^\circ, 3^\circ, 42^\circ$ in August 2012. Legend: Black line – *In situ*; Blue line – New model; Red line – Model 1 [15]; Green line – Model 2 [18].

Figures 10 and 11 show the variations of the model and *in situ* K_d for different wavelengths and depth layers at the time-series station [Fig. 10] and discrete stations [Fig. 11] off Point Calimere before and during the southwest monsoon (May 2012 and August 2012). At many stations, the K_d values derived from the new model are consistent with the *in situ* K_d values, and both these K_d profiles tend to increase with increasing depth and become more prominent at the bottom layers due to the contribution of scattering. A slight deviation of the modeled K_d at this layer may be attributed to inelastic scattering which is not explicitly

determined and included in our study (because the internal sources caused by Raman scattering and chlorophyll fluorescence cannot be discriminated from each other by radiometric measurements). In fact, a fraction of this deviation may also be caused by the additional unqualified error caused by small-scale vertical and horizontal variability in the water column optical properties (considering the timing of the deployment of WETLAB sensors and Trios sensors, with a deployment interval of 10 minutes apart) in the dynamic coastal ocean.

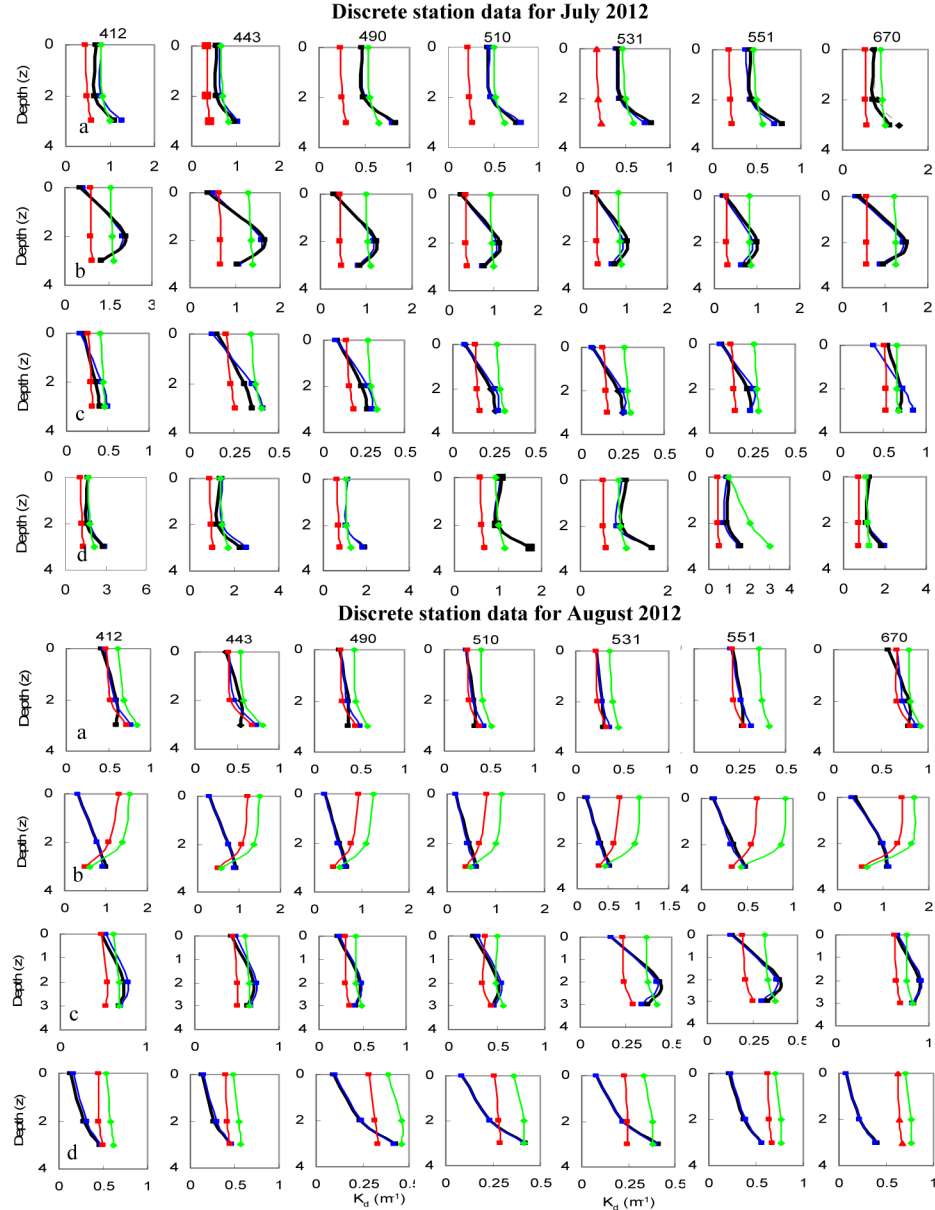


Fig. 11. Comparison of the modeled $K_d(\lambda)$ with *in situ* $K_d(\lambda)$ for different depth layers (z) at the discrete coastal stations (a-d correspond to St-1, St-2, St-3 and St-4) off Point Calimere before and during the southwest monsoon (May 2012 and August 2012). Black line – *In situ*; Blue line – New model; Red line – Model 1 [15]; Green line – Model 2 [18].

Nevertheless, the observed variability in K_d is associated with the IOP variability attributed to tides, alongshore currents and winds and changes in incident solar radiation. Under these prevailing conditions, the K_d profiles obtained with the existing models are not generally agreeable with the *in situ* K_d profiles from both relatively clear and highly turbid coastal waters (For brevity the profile comparisons not shown for clear waters off Chennai).

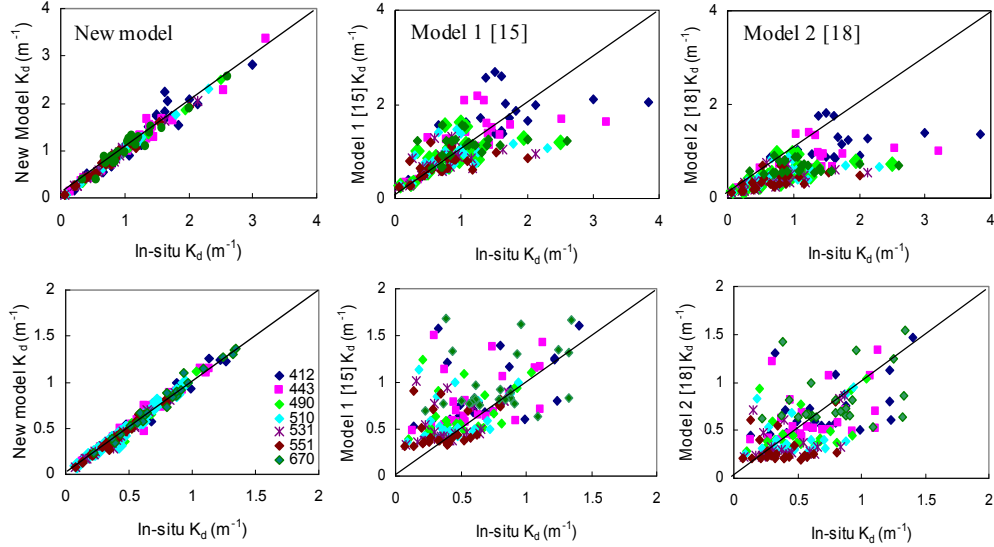


Fig. 12. Comparison of the modeled $K_d(\lambda)$ values from the new model and existing models with *in situ* $K_d(\lambda)$ values at some key wavelengths (412, 443, 490, 510, 531, 551 and 670 nm) ($N = 58$) (Top panels – Before the southwest monsoon; Bottom panels – During the southwest monsoon).

To better illustrate the performance of the new model and existing models, Fig. 12 shows the modeled and *in situ* K_d data at some key wavelengths from three cruises (including data from three depth layers and for different solar zenith conditions). The new model has nearly identical results compared to the *in situ* data. Further, the error plots confirm that the important feature of the new model is its stability whatever the wavelengths being considered [Fig. 13]. In particular, the RMSE, MRE, Bias and Intercept values associated with the new model are apparently closer to zero and slope and R^2 values are closer to unity. These low errors and high slope and R^2 values indicate that there is good agreement between the model and measurement data. Not surprisingly, the existing models produce inaccurate K_d data that are highly scattered (overestimation or underestimation) above and below the 1:1 line with respect to the measured data. As a result, their errors are not only very high but fluctuating across the wavelengths (indicating poor performance of these models). These results suggest that the new model is very promising in reproducing measured K_d values across the entire visible wavelengths and for different solar zenith and in-water optical conditions in both clear and highly turbid coastal waters.

6. Relationship between $K_d(360)$ and $K_d(490)$ for ocean optics and remote sensing

Many studies have been carried out in the past decades to acquire knowledge of ultra-violet (UV) radiation penetration which is important for the study phytoplankton dynamics [43, 44], quantifying the photoreaction rates of DOM in the water column [45], understanding coral bleaching in shallow waters. Past studies derived simple relationships by relating CDOM absorption or DOC (dissolved organic carbon) to K_d , which take into account the contributions of the absorption coefficient to K_d but eventually ignore the contributions of the backscattering coefficient. Experimental and modeling studies have shown that the magnitude

of backscattering for relatively clear and turbid coastal waters (particle-rich waters) could be much larger in the short wavelength region [46].

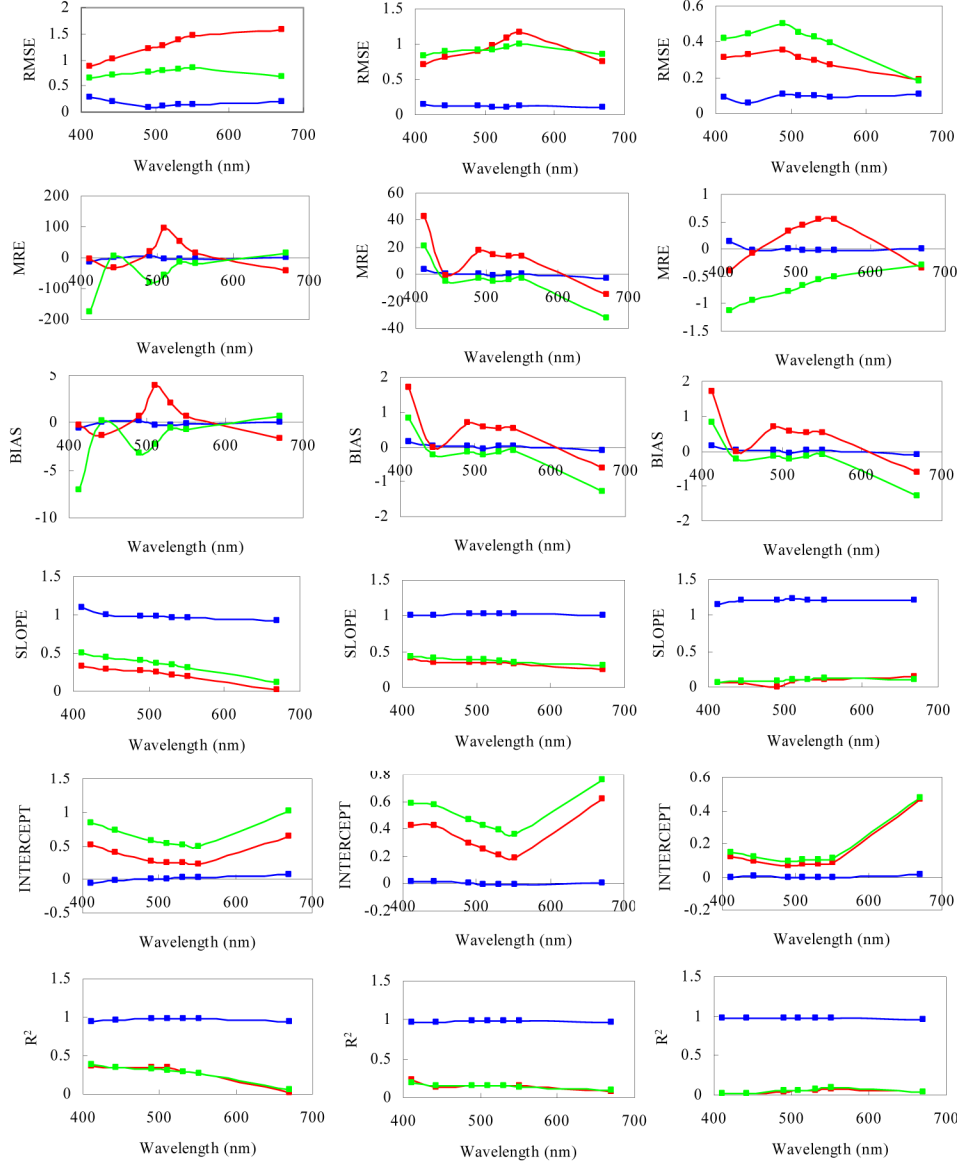


Fig. 13. Statistical comparisons between the modeled and measured K_d values in clear and turbid coastal waters off Point Calimere and Chennai before and during the southwest monsoon (all three cruises data used for this analysis). RMSE – root mean square error and MRE – mean relative error. Legend: Blue – New model; Red – Model 1 [15]; Green – Model 2 [18].

To quantify and understand the penetration of the light, the depth ($Z(360)_{10\%}$) corresponding to 10% of its surface values [47] is calculated from $K_d(360)$ (i.e., $Z(360)_{10\%} = 2.3 / K_d(360)$). If one calculates $K_d(360)$ analytically, the a and b_b coefficients (at 360nm) should be derived from R_{rs} -IOPs inversion methods, where $R_{rs}(360-400)$ is usually measured *in situ* since the present satellite sensors do not provide this quantity directly. To

overcome this limitation, $K_d(360)$ is related to $K_d(490)$ by the following relationship derived from Fig. 14.

$$K_d(360) = 0.0386 + 1.6034K_d(490); R^2 = 0.77. \quad (23)$$

where $K_d(490)$ can be estimated from satellite measurements with good accuracy [10]. Note that we use the wavelength 490 for the estimation of $K_d(360)$, since our experimental and modeling study shows that the impact of solar zenith and water's IOPs on estimating $K_d(490)$ is minimum and its estimation accuracy is significantly higher at this wavelength [10]. Lee et al. [9] provided a similar relationship for a lower (restricted) range of $K_d(360)$ values ($0.02\text{--}0.08 \text{ m}^{-1}$) that is applicable only for clear oceanic waters. The proposed method [Eq. (23)] would be useful for satellite application studies as well, to know the UV radiation availability in the water column and their spatial and temporal distributions in global coastal oceanic waters.

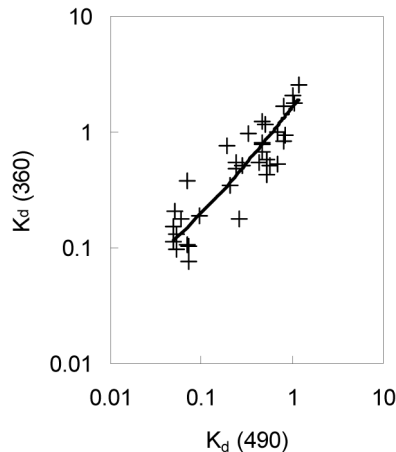


Fig. 14. Relationship between *in situ* $K_d(360)$ and $K_d(490)$ values from the profile measurements obtained in relatively clear and turbid coastal waters off Point Calimere and Chennai during before and during the southwest monsoon.

7. Discussion and conclusions

Several empirical and semianalytical models are often used to derive K_d based on satellite measurements and IOPs measured *in situ* or stimulated [17, 48–53]. K_d is a significant parameter for precise assessment of the light intensity at depth [54] and classifying water types [1]. For the vast ocean, satellite remote sensing plays an important role to obtain repetitive and fine-scale measurements of K_d . However, many algorithms which depend on the blue-green ratio of radiances or reflectances were found to overestimate or underestimate $K_d(490)$ values in both clear and turbid waters where the backscattering caused by suspended matters and the absorption by dissolved organic matters increase light attenuation in the water column. Many empirical relationships are used to estimate values of K_d from remotely sensed data by relating K_d and the spectral ratio of water leaving-radiance at two wavelengths [26, 27]. However, these algorithms suffer from large uncertainties in the derived products [10], and are insufficient to enhance our present understanding of the vertical spectral distributions of K_d in turbid coastal waters [17, 50]. Many of these models are generally applicable for waters with low particle concentrations. Recently, Wang et al. [40] developed a new K_d model by relating the backscattering coefficient at the wavelength 490nm to the irradiance reflectance just beneath the surface at the red wavelength. Though this K_d model is applicable for turbid waters, it is merged with the standard models so as to find its applicability in both clear and turbid waters.

Many semianalytical approaches based on radiative transfer simulations have also been developed that provide the relationship between $K_d(z)$ and IOPs [2, 8, 9, 15–18, 40, 55]. While the empirical algorithms suffer from large uncertainty and are insufficient to provide a better understanding of the spatial and temporal variability of K_d , these semianalytical approaches overcome such limitations by improving the accuracy of K_d but are valid only for limited sky and oceanic conditions and are generally applicable to clear and moderately turbid waters. Lee et al. [8] developed a K_d model for vertically homogenous water based on the radiative transfer modeling results, where the model parameters are derived from Hydrolight simulations using the particle phase function under clear sky conditions and wind speed of 5 m s⁻¹. It means that further refinement is required for cloudy conditions and high wind speed conditions. Parameterizations of the modeled values are obtained from Look-up tables, which are not appropriate for all water conditions. However, challenges remain to extend the models to vertically stratified waters. On the other hand, the formula [Eq. (4)] proposed by Kirk [18] underestimates $K_d(z)$ and finds difficulty to parameterize the appropriate coefficients associated with the scattering phase function. As the field data used were collected from waters with medium particles (Chl <3mg m⁻³) and medium solar position ($\theta <60^\circ$), approximation of parameter values was done by calculating average K_d from surface to depth receiving 1% and 10% of surface irradiance. Such approximations fail especially in turbid waters.

Based on the asymptotic closure theory [29, 56, 57], K_d at relatively high solar position is derived. These models may become rapidly invalid when solar elevation is low. However, a more complicated asymptotic closure model was developed by McCormick [58], but deriving the parameters from IOPs and solar elevation remains extremely difficult. Although the Eq. (7) has been widely accepted and applied to ocean optics, it fails (underestimates K_d) in particle rich waters because of the dominance of scattering effect. It works better for upper layer than for lower layer. Though several models are available to estimate K_d , none of these models provide K_d values over the entire visible spectral bands. Estimation of K_d over the entire wavelength is necessary for many applications – including classification of waters, classification of algal blooms, estimation of light intensity at depth, the study of heat budget [6, 7, 59, 60] and photosynthesis [3, 34, 61].

To overcome many of these limitations, a new diffuse attenuation coefficient model $K_d(z, \lambda, \theta)$ has been developed and systematically evaluated using the *in situ* data obtained from turbid waters off Point Calimere (where the water properties are highly dominated by high levels of suspended sediments, detrital particles and phytoplankton) and relatively clear waters off Chennai. The new model has been derived based on the absorption and backscattering coefficients for the entire visible wavelength range (400-700nm), different depth layers (surface, intermediate and bottom layers) and varying zenith angles. On the basis of extensive analysis of field data, the values of the model parameters have been derived by fitting the data with the model. The model parameters vary with solar zenith angle, depth and b_b/a . The results of the new model have been compared with the *in situ* K_d profiles for different depths, solar zenith angles and wavelengths. It is found that the new K_d model is valid for both relatively clear and turbid coastal waters. Its applicability has also been assessed in waters with low, medium and particle concentrations (where Chl ranges from ~0.1 to 13 µg L⁻¹) and for varying solar zenith angles (morning to evening). The new model is found to be valid in these waters characterized by the overall range of a (0.12m⁻¹ ~1.118m⁻¹), b_b (0.001 m⁻¹ ~0.3 m⁻¹) and turbidity (~0.44-16 NTU). Compared to the existing models whose results are highly fluctuating (overestimation or underestimation) for different wavelengths, depth layers, water types and solar zenith conditions, the model has definitely improved the accuracy of K_d in both relatively clear and turbid coastal waters (percent MRE between the model and *in situ* measurements being less than 13.34%, other errors being very small and R² always >0.94). Since the new K_d model yields accurate K_d values for the entire visible spectrum (400-700 nm) and different depth layers in both clear and turbid waters, it can be applied to a wide range of coastal oceanic waters.

A thorough evaluation of the results demonstrates that the new model has higher capability in both relatively clear and highly turbid waters. It provides a rapid method to obtain the vertical spectral distributions of K_d from IOPs measurements with significantly higher accuracy, thereby offering improvement over other models in both relatively clear and highly turbid waters within the coastal oceanic domain. It may be extended for satellite applications, but its accuracy depends significantly on the inverse retrievals of IOPs from R_{rs} by empirical or semianalytical algorithms. The new model will have important implications for understanding ocean physics, biogeochemical cycles, and underwater applications in highly dynamic coastal oceanic waters.

Acknowledgments

This work was supported by grants from the NRB (Project Number OEC1112106NRBXPSHA). This work was also supported by IIT Madras, Chennai-600036. We would like to thank D. Rajasekhar, The Head, Vessel Management Cell (VMC), and Director of National Institute of Ocean Technology (NIOT) for providing the Sagar Purvi and Sagar Pachimi (Coastal Research Vessels) to Indian Institute of Technology (IIT) Madras, Chennai, India for making various bio-optical and underwater light field measurements. We thank Scientists N. Ravi and K Shashikumar for arranging the vessels on time and other members of VMC for their help during the *in situ* measurements. We are thankful to the anonymous reviewers for the valuable comments, which helped to improve the quality of the manuscript.